Table 1. NBI of lesions in the squamous epithelium of the head and neck region and the esophagus

Year	First author	Objective	NBI system	Endoscope	Magnification	NBI findings	Ref. no
2004	Muto	Diagnosis of superficial cancer in the oropharynx and hypopharynx	RGB sequential illumination system	Gastrointestinal endoscope	+	1. Well-demarcated brownish area; 2. microvascular proliferation pattern	15
2004	Yoshida	Diagnosis of superficial esophageal lesions	RGB sequential illumination system	Gastrointestinal endoscope	+	RGB band value of IPCL and background mucosa	14
2005	Muto	Diagnosis of superficial cancer in the oropharynx and hypopharynx	RGB sequential illumination system	Gastrointestinal endoscope	+	NBI improved identification of brownish area and microvascular irregularity	4
2006	Watanabe	Diagnosis of superficial cancer in the oropharynx and hypopharynx	Color CCD chip system	Rhinolaryngoscope	–	NBI laryngoscope can detect carcinoma in situ	16
2007	Lee	Grading of esophagitis	RGB sequential illumination system	Gastrointestinal endoscope	–	NBI improved intraobserver and interobserver consistency	21
2007	Sharma	Diagnosis of GERD	RGB sequential illumination system	Gastrointestinal endoscope	+	Increased number and dilation of IPCLs are the best predictors	20
2008	Watanabe	Diagnosis of superficial cancer in the oropharynx and hypopharynx	Color CCD chip system	Rhinolaryngoscope	–	NBI improved accuracy, sensitivity, and negative predictive value	17

NBI, narrow-band imaging; IPCL, intrapapillary capillary loop; GERD, gastroesophageal reflux disease; RGB, red-green-blue; CCD, charge-coupled device

Gastroesophageal reflux disease

Gastroesophageal reflux disease (GERD) is a common disorder causing heartburn in Western countries. Patients are endoscopically classified as having non-erosive reflux disease (NERD), erosive esophagitis, or Barrett's esophagus. Because more than 60% of patients with GERD show no signs of esophagitis, NERD is also described as endoscopy-negative reflux disease. In some ways, conventional endoscopy is a rather insensitive test for the diagnosis of GERD in patients with NERD. Kiesslich et al.[19] reported that patients with NERD show a prominent vasculature pattern above the Z-line, although they found no significant difference between NERD patients and the control group. NBI is expected to overcome the limitations of conventional endoscopy and allow the visualization of superficial and small esophageal lesions in GERD patients that cannot be seen by conventional white light endoscopy.

Sharma et al.[20] conducted a feasibility study of NBI with a magnifying endoscope (GIF-Q240Z, Olympus Medical Systems) in patients with GERD. GERD symptoms were evaluated by two validated questionnaires. The features seen only by NBI were compared between GERD patients and controls. Patients with GERD had increased numbers, dilation, and tortuosity of IPCLs compared with controls. Multivariate analysis showed that increased numbers and dilation of IPCLs were the best predictors of a diagnosis of GERD. Therefore, they concluded that NBI endoscopy might improve the diagnosis of GERD, particularly in patients with NERD. The results of this pilot study indicate that NERD should be reevaluated by novel technologies in a prospective controlled trial.

Using high-resolution endoscopy (GIF-H260, Olympus Medical Systems), Lee et al.[21] reported that NBI improved intraobserver and interobserver reproducibilities in grading esophagitis compared with conventional white light imaging. In this study, the Los Angeles classification was used for evaluation of esophagitis. The Los Angeles classification was originally established to improve intraobserver and interobserver agreement. However, evaluation of mucosal breaks depends on the observer's experience in performing upper endoscopy and thus often results in poor to fair agreement. NBI is useful for overcoming these difficulties in grading esophagitis.

Interobserver and intraobserver consistency are important for standardization of accurate diagnoses. In the Kansas study,[20] intraobserver agreement was modest, while interobserver agreement was very good, perhaps because of the limited number of investigators (only two) and the time required to learn to recognize novel IPCL findings in GERD. Thus, the problem of interobserver and intraobserver variability might be solved

by shortening the learning curve with the use of magnifying endoscopy.

Barrett's esophagus

Barrett's esophagus is defined as the presence of columnar epithelium in the distal esophagus with histological evidence of specialized intestinal metaplasia (SIM). The most important risk factor for development of Barrett's esophagus is chronic acid reflux disease, which stimulates the replacement of the distal esophageal squamous epithelium with SIM. Barrett's esophagus is a precursor of esophageal adenocarcinoma, and endoscopic surveillance has therefore been recommended to detect intraepithelial neoplasia or adenocarcinoma at an early stage such as mucosal cancer. Table 2 summarizes published data about Barrett's esophagus.

However, with conventional white light endoscopy it is difficult to identify dysplastic and early neoplastic changes in SIM. In Western countries, use of four-quadrant random biopsies is widely accepted, but they are prone to sampling error because it is a "blind approach." Improvement of visualization of Barrett's columnar epithelium and distinguishing metaplasia from dysplasia or neoplasia is expected to result in more accurate biopsies and more effective screening.

Hamamoto et al.[22] were the first to report that NBI is able to provide better visualization of the esophagogastric junction, net-like capillary vessels, and the columnar-lined esophagus than conventional white light endoscopy. Using high-resolution endoscopy, Kara et al.[23] conducted a prospective randomized crossover study comparing indigo carmine chromoendoscopy to NBI for the detection of high-grade dysplasia or early cancer in patients with Barrett's esophagus. Among 28 patients with known or suspected high-grade dysplasia or early cancer, 14 were histologically confirmed by targeted or random biopsies. The overall sensitivity for diagnosis of high-grade dysplasia and early cancer was comparable between indigo carmine chromoendoscopy (93%) and NBI (86%). Most lesions could be identified by high-resolution endoscopy alone (79%), suggesting that NBI might replace indigo carmine chromoendoscopy as an adjunct to high-resolution endoscopy.

NBI with magnifying endoscopy enables visualization of the details of the mucosal surface and capillary networks without using dyes. Characteristics of SIM observed by high-resolution endoscopy with NBI are a regular villous/gyrus-forming pattern and a regular vascular pattern.[24,25] High-grade intraepithelial neoplasia is characterized by three abnormalities: an irregular/disrupted mucosal pattern, an irregular vascular pattern, and abnormal blood vessels. All high-grade intraepithelial neoplasia have at least one abnormality, and 85% have two or more abnormalities.[24] These criteria are quite accurate for the diagnosis of SIM and high-grade intraepithelial neoplasia, respectively. Goda et al.[26] reported that the addition of a capillary pattern to fine mucosal patterns improved the diagnostic value of observations by magnifying endoscopy with NBI for detecting SIM and superficial adenocarcinoma. Kara et al.[24] also reported the importance of the vascular pattern for recognizing dysplastic and cancerous lesions in Barrett's esophagus.

Most studies evaluate the mucosal pattern and capillary pattern separately.[24–26] Each type of data is very important for understanding the details of both subtle mucosal changes and irregular microvascular changes, in particular their clinical significance. However, these classifications are difficult to apply in routine clinical practice. To reduce interobserver variability, a simple classification system is important.

Anagnostopoulos et al.[27] reported the diagnostic power of using both mucosal and capillary patterns for detection of SIM and high-grade dysplasia. Sensitivity, specificity, and positive and negative predictive values for the combination of a regular microstructure pattern (tubular/villous/linear) and no microstructural pattern to detect SIM were 100%, 78.8%, 93.5%, and 100%, respectively, and those for the combination of an irregular microstructure pattern and the presence of a microvascular pattern for prediction of high-grade dysplasia were 90%, 100%, 99.2%, and 100% respectively.

Singh et al.[28] simplified the grading system for mucosal morphology patterns in relation to histology as follows: type A, round pits with regular microvasculature (columnar mucosa without intestinal mucosa); type B, villous/ridge pits with regular microvasculature (intestinal metaplasia); type C, absent pits with regular microvasculature (intestinal metaplasia); and type D, distorted pits with irregular microvasculature (high-grade dysplasia). The positive and negative predictive values were 100% and 97%, respectively, for type A (columnar mucosa without intestinal mucosa); 88% and 91%, respectively, for types B and C (intestinal metaplasia); and 81% and 99%, respectively, for type D (high-grade dysplasia). This classification showed reproducibility and repeatability both by endoscopists experienced in the use of NBI and those unfamiliar with NBI, suggesting a rapid learning curve. Therefore, NBI combined with high-resolution magnifying endoscopy allows both expert and nonexpert endoscopists to perform targeted biopsies for SIM and high-grade dysplasia with high success.

In contrast, Curvers et al.[29] reported that the addition of enhancement techniques, including indigo carmine chromoendoscopy, acetic acid chromoendoscopy, and NBI to white light imaging did not improve

Table 2. NBI for Barrett's esophagus

Year	First author	NBI system	Magnification	Study aim and evaluation	Results	Ref. No
2004	Hamamoto	RGB sequential illumination system	+	Visualization of Barrett's esophagus	NBI > WLI	22
2005	Kara	RGB sequential illumination system	+	Detection of high-grade dysplasia and early cancer	Indigo carmine chromoendoscopy = NBI	23
2006	Sharma	RGB sequential illumination system	+	Ridge/villous pattern for diagnosis of intestinal metaplasia	Sensitivity (93.5%), specificity (86.7%), positive predictive value (94.7%)	25
				Ridge/villous pattern for diagnosis of high-grade dysplasia	Sensitivity (100%), specificity (98.7%), positive predictive value (95.3%)	
2006	Kara	RGB sequential illumination system	+	Characterization and classification of mucosal morphology	SIM: 80% = villous/gyrus-forming pattern with regular vascular pattern 20% = flat mucosa with normal-appearing long branching vessels High-grade intraepithelial neoplasia: irregular/disrupted mucosal pattern, irregular vascular pattern, abnormal vessels	24
2007	Anagnostopoulos	RGB sequential illumination system	+	Irregular microvascular/microstructural pattern for the prediction of high-grade dysplasia	Sensitivity (90%), specificity (100%), negative predictive value (99.2%), negative predictive value (100%)	27
2007	Goda	RGB sequential illumination system	+	Comparison of mucosal pattern and capillary pattern	SIM: cerebriform fine mucosal pattern, ivy- or deoxyribonucleic acid-like capillary pattern mucosal pattern + capillary pattern improve the diagnostic accuracy of SIM	26
2008	Wolfsen	Color CCD chip system	–	Detection of high-grade dysplasia	NBI > WLI	30
				Grade of dysplasia	NBI > WLI	
				Number of biopsy sample	NBI < WLI	
2008	Curvers	RGB sequential illumination system	+	Interobserver agreement for the mucosal morphology (indigo carmine chromoendoscopy vs. acetic acid chromoendoscopy vs. NBI)	No difference	29
			+	Identification of early neoplasia (indigo carmine chromoendoscopy vs. acetic acid chromoendoscopy vs. NBI)	No difference	
2008	Singh	RGB sequential illumination system	+	Type A (round pits with regular microvasculature)	Positive predictive value (100%), negative predictive value (97%)	28
				Type B (villous/ridge pits with regular microvasculature)	Positive predictive value (88%), negative predictive value (91%)	
				Type C (absent pits with regular microvasculature)	Positive predictive value (88%), negative predictive value (91%)	
				Type D (distorted pits with regular microvasculature)	Positive predictive value (81%), negative predictive value (99%)	

SIM, specialized intestinal metaplasia; WLI, white light imaging

interobserver agreement with regard to neoplasia in Barrett's esophagus. Interpretation of their study has some limitations because they used a smaller number of the photos than other studies, and they used only the best still photos that they obtained, selected on the basis of image quality and similarity. These still photos were a set comprising indigo carmine chromoendoscopy, acetic acid chromoendoscopy, NBI, and white light imaging photos. During routine endoscopic observation, it is sometime difficult to obtain high-quality images because of, for example, excess dye, unevenly spread dye, or contact bleeding. As a result, it may be difficult to make a real-time or on-site endoscopic diagnosis. Therefore, their negative results might have been caused by selection bias. In other words, this study reveals the importance of image quality and comparability among images for accurate diagnosis and good interobserver agreement. In the near future, we should ascertain the actual and real-time yield of enhancement techniques for identifying neoplasia to improve the clinical practice.

All of these endoscopic studies of Barrett's esophagus except one used an RGB sequential illumination system, and most studies were carried out in Western countries. This may suggest that RGB sequential illumination system is superior to the color chip system when NBI and magnifying endoscopy are combined. Using a color chip system, Wolfsen et al.[30] compared high-resolution NBI endoscopy with conventional resolution white light endoscopy. They showed an increased yield with the use of high-resolution NBI compared with the use of conventional resolution white light endoscopy, as well as a need for fewer biopsies.[30] In addition, high-resolution NBI detected higher grades of dysplasia in individual patients and detected dysplasia in more patients compared than conventional resolution endoscopy. These findings suggest that a difference in the videoendoscopy system may not be very important in terms of diagnostic power and that NBI is no longer the standard for detecting high-grade dysplasia and superficial cancer in Barrett's esophagus.

Stomach

In the stomach, NBI should be used during magnifying endoscopy observation. Because light intensity under the NBI filter is low, the nonmagnified image is darker than the white light image. Furthermore, if electronic enhancement is used to brighten the endoscopic image, the image becomes noisy. Thus, nonmagnifying endoscopy is insufficient to observe the wide space of the stomach. In inexperienced hands, the endoscopic diagnosis might be misleading and lesions might be overlooked. Table 3 summarizes the published data on

Table 3. NBI for gastric lesions

Year	Author	NBI system	Magnification	Evaluated lesions	NBI findings	Ref. No
2004	Nakayoshi	RGB sequential illumination system	+	Differentiated adenocarcinoma	Fine network pattern	34
				Undifferentiated adenocarcinoma	Corkscrew pattern	
2004	Sumiyama	RGB sequential illumination system	+	Gastric cancer	Irregular fine network capillary structure	35
					Border of lesion recognized by differences in capillary structure	
2006	Tamai	RGB sequential illumination system	+	Depressed gastric adenoma	Regular ultrafine network pattern	36
2006	Uedo	RGB sequential illumination system	+	Gastric intestinal metaplasia	Light blue crest	31
2007	Yao	RGB sequential illumination system	+	Differentiated adenocarcinoma	Demarcation line	
					Disappearance of regular subepithelial capillary network pattern	33
					Irregular microvascular pattern	
2008	Bansal	RGB sequential illumination system	+	Normal epithelium/ mild-moderate gastritis	Regular mucosal and capillary pattern	
				H. pylori gastritis	Irregular mucosal pattern and decreased capillary density	32
				Intestinal metaplasia	Ridge/villous mucosal pattern	

gastric lesions. All studies but one were reported by Japanese researchers.

Identification of intestinal metaplasia by NBI

Helicobacter pylori-associated gastritis induces atrophic gastritis and intestinal metaplasia (IM) and is a risk factor for dysplasia and gastric cancer. Gastric IM is associated with a risk for the development of differentiated adenocarcinoma. However, conventional white light imaging has a high rate of interobserver variability and correlates poorly with histological findings. Uedo et al.[31] first found that in magnifying NBI, the appearance of a light blue crest in the gastric mucosa is a highly accurate indicator of the presence of histological metaplasia. Bansal et al.[32] also reported that the sensitivity and specificity of a ridge/villous pattern for the diagnosis of intestinal metaplasia are 80% and 100%, respectively.

Differential diagnosis of superficial gastric cancer

To date, there is no evidence that magnifying NBI is superior for the detection of an early gastric neoplasm compared with magnifying white light imaging. Conventionally, an endoscopic diagnosis of a superficial gastric neoplasm is made on the basis of mucosal surface structural and color changes. However, there is high interobserver variability in the identification of these changes, so accurate diagnosis of superficial gastric cancer is quite difficult, especially for nonexpert endoscopists.

Yao et al.[33] reported unique magnifying endoscopy findings in intestinal-type gastric cancer as follows: (1) presence of a demarcation line between the reddish lesion and the surrounding mucosa; (2) disappearance of the regular subepithelial capillary network (SECN); and (3) presence of an irregular microvascular pattern within the flat lesions. They prospectively studied the diagnostic accuracy of these magnifying endoscopy findings for differentiating between gastritis and flat, reddish gastric cancer. All of the gastric cancer lesions showed both the demarcation line and the disappearance of the regular SECN, whereas only 25.3% and 22.9% of gastritis lesions showed these findings. The sensitivity and negative predictive value of the demarcation line and the disappearance of the regular SECN for distinguishing flat gastric cancer were both 100%. The diagnostic accuracy of an irregular microvascular pattern was 98.7%. Therefore, magnifying endoscopy findings based on microsurface and microvascular architecture are quite useful for making a differential diagnosis between flat reddish gastric cancer and gastritis.

As a next step, we should investigate the reproducibility of the results and compare the yield of gastric cancer between magnifying NBI and magnifying white light imaging in a randomized controlled study, because NBI is known to strongly enhance visualization of microsurface and microvascular architecture.

Nakayoshi et al.[34] classified the microvascular pattern of superficial gastric cancer in magnifying NBI images into three groups: A, fine network, B, corkscrew, and C, unclassified patterns. They also compared endoscopic patterns with histological findings. Among 109 cases of differentiated early gastric adenocarcinoma, microvascular patterns A, B, and C were observed in 66%, 3.7%, and 30.3% of cases, respectively. In contrast, among 56 cases of undifferentiated early gastric adenocarcinoma, pattern B was observed in 85.7% of cases, whereas patterns A and C were observed in 3.6% and 10.7%, respectively. Thus, the microvascular pattern in magnifying NBI images is useful for predicting the histologic type of superficial gastric cancer: differentiated adenocarcinomas display a fine network pattern, whereas undifferentiated adenocarcinomas display a corkscrew pattern in their microvascular structure.

Magnifying NBI is also useful for identifying the lateral extent of superficial gastric cancer.[35] This capability is very important for accurate assessment of the safety margin, to ensure complete resection by EMR or ESD.

Gastric adenoma

Most gastric adenomas are the protruded type. While depressed-type adenomas are rare, they are clinically important because they have higher malignant potential than protruded adenomas. However, detection of depressed-type adenomas has been difficult because endoscopic findings have not been clearly defined. Tamai et al.[36] reported that depressed-type adenomas display a regular ultrafine pattern, in which the network of microvessels is composed of small, regular circles. This pattern differs from the irregular fine network pattern of well-differentiated adenocarcinomas.

Duodenum

Ampullary tumor is a relatively rare neoplasm and is an indication for endoscopic or surgical resection. However, the selection of treatment remains controversial, because the differential diagnosis between adenoma and adenocarcinoma is difficult. Therefore, an accurate diagnosis is needed so that the appropriate management for the patient can be selected. Uchiyama et al.[37] reported that inflammatory changes result in oval-shaped villi, whereas all adenomas and adenocarcinomas display pinecone/leaf-shaped villi, or an irregular, nonstructured pattern. Similar to superficial cancer of

Table 4. Comparison of diagnostic performance for neoplastic and nonneoplastic lesions between conventional colonoscopy, chromoendoscopy, and NBI

Year	First author	Evaluation methods	*n* (lesions)	Endoscopy system	Magnification	Modality	Sensitivity	Specificity	Accuracy	Ref. No
2004	Machida	Real-time diagnosis	43	RGB sequential illumination system	+	Conventional WLI	85.3	44.4	79.1	5
						Chromoendoscopy	100	75	93.4	
						NBI	100	75	93.4	
2007	Su	Blinded review of recorded DVD	110	RGB sequential illumination system	–	Conventional WLI	82.9	80	72.7	44
						Chromoendoscopy	95.7	87.5	92.1	
						NBI	95.7	87.5	92.1	
2007	Chiu	Blinded review of selected images with best quality	180	RGB sequential illumination system	–	Conventional WLI	62.1–65.2	74.4–85.4	67.2–68.3	45
						Chromoendoscopy	78.7–85.1	79.5–84.6	78.9–85.0	
						NBI	82.3–86.5	59–82.7	80.6–82.4	
					+	Chromoendoscopy	91.3–97.2	74.4–90.5	92.2–91.1	
						NBI	87.0–95.0	71.8–88.1	87.2–90.0	

the esophagus, magnifying NBI can be used to predict the histological characteristics of an ampullary lesion. Abnormal vessels are seen only in adenocarcinomas and not in adenomas.

Colon

Most colorectal cancers (CRCs) arise from adenomas, according to the adenoma-carcinoma sequence concept.[38] Therefore, early detection and subsequent removal of adenomas are very important to reduce the incidence of CRC and the consequent mortality. However, it is sometimes difficult to distinguish neoplastic (adenoma with dysplasia and adenocarcinoma) from nonneoplastic polyps (e.g., hyperplastic polyps) by conventional white light imaging. Nonneoplastic lesions, which do not require removal, account for 10%–30% of removed polyps.[39] Furthermore, a systematic review of published data reported that 22%–28% of adenomas may be missed during colonoscopic screening.[40–42] Chromoendoscopy using a dye such as indigo carmine (dye-based image enhanced endoscopy) increases the detection rate of small flat or depressed lesions, which have a higher malignant potential than protruding ones. Fu et al.[43] reported that magnifying chromoendoscopy is significantly better than chromoendoscopy alone or white light imaging alone for the diagnosis of neoplastic lesions. NBI has the potential to decrease the number of overlooked lesions and the number of lesions unnecessarily removed.

Distinguishing neoplastic from nonneoplastic lesions with conventional colonoscopy, chromoendoscopy, and NBI

Machida et al.[5] first evaluated the clinical feasibility of the NBI system for colorectal lesions. In their pilot study, NBI with a magnifying endoscope achieved better visualization of the mucosal vascular network pattern than conventional white light imaging. They found that the diagnostic accuracy of NBI for neoplastic polyps was equivalent to that of chromoendoscopy. Furthermore, and of clinical relevance, their data were obtained by real-time image processing during colonoscopy, whereas most other studies used have used recorded images and, what is more, only selected excellent images. Su et al.[44] reported similar results with NBI but without the use of a magnifying endoscope. Chiu et al.[45] demonstrated that both low- and high-magnification NBI is capable of distinguishing neoplastic from nonneoplastic lesions, and that its diagnostic accuracy is better than that of conventional white light imaging and equivalent to that of chromoendoscopy (Table 4).

All three studies used an NBI endoscopy system based on RGB sequential illumination (CF-Q240ZI, Olympus Medical Systems) and showed that NBI could distinguish neoplastic from nonneoplastic colorectal lesions, indicating that NBI, with either magnifying or nonmagnifying endoscopy, has the potential to replace dye-based chromoendoscopy for this purpose.

NBI for detection of colorectal adenoma

Rex et al.[46] compared white light imaging and NBI in a prospective randomized controlled trial of colonoscopy withdrawal for colorectal adenoma detection. In their study, a single endoscopist used a high-definition but nonmagnifying colonoscope based on the color CCD system (Olympus 180 series, Olympus America, Center Valley, PA, USA). They found that NBI did not result in a high adenoma detection rate. Using same model of nonmagnifying colonoscope, Adler et al.[47] also reported negative results for adenoma detection by NBI compared with conventional white light imaging.

In colonoscopic screening, overlooking of the colon polyp is one of the major problems to be solved, because it can lead to the development of colon cancer within a few years after a complete colonoscopy. Rastogi et al.[48] demonstrated in their back-to-back study that a second NBI pass detected more adenomas than the first pass with white light colonoscopy. However, their study has several limitations. Patients were not randomized to either the conventional and NBI colonoscope, and 40% of the additional polyps could be detected by a second white light colonoscopy. Furthermore, the study was a pilot feasibility study so the results are not definitive.

In hereditary nonpolyposis colorectal cancer (HNPCC), colonic adenoma appears to show accelerated progression to carcinoma.[49] Thus, colonoscopic surveillance is very important to reduce the death rate.[50] In a back-to-back study, East et al.[51] reported that a second pass with NBI of the proximal colon of HNPCC patients detected significantly more adenomas than the first pass with white light colonoscopy. In addition, the proportion of flat adenomas detected was higher in the NBI pass than in the white light pass. These results indicate that NBI can help reduce interval cancer rates.

In a recent prospective randomized controlled study in Japan, Inoue et al.[52] detected significantly more adenomas and more diminutive (<5 mm) lesions with a pancolonic NBI system than with conventional white light imaging. They used an endoscope based on the RGB sequential illumination system, but it is not clear whether they used a magnifying endoscope.

Flat and depressed colorectal neoplasia are difficult to identify with conventional white light colonoscopy. Uraoka et al.[53] conducted a pilot single-center study and reported that NBI improved the detection of flat and diminutive lesions over conventional white light imaging.

At present, NBI has been shown to be useful for detection of colonic adenoma only by studies using magnifying NBI and the RGB sequential illumination system (Table 5).

Identification of pit patterns and vascular patterns by NBI

Kudo et al.[54] proposed a pit pattern classification system using chromoendoscopy that has been widely accepted by experienced endoscopists. This classification system shows excellent sensitivity of more than 90% relative to histologic diagnosis. Interobserver and intraobserver variabilities are also low. Magnifying NBI can enhance the mucosal surface pit pattern without dye staining or spraying.[5] East et al.[55] reported that pit patterns are not always identical between NBI and conventional chromoendoscopy, as assessed by two experienced endoscopists, one Japanese trained and the other European trained. They proposed that the classification system of Kudo et al.[54] should be modified and validated before it is used. In contrast, Hirata et al.[56] reported that determination of the pit pattern by NBI with magnification was nearly the same as that obtained by standard magnification with chromoendoscopy. However, their study was a retrospective analysis, and, furthermore, the image assessment method used is unclear.

With regard to the vascular pattern, Katagiri et al.[57] demonstrated that the capillary pattern detected by magnifying NBI can be used to assess the degree of atypia in early colorectal neoplasia. This pilot study was performed by a single endoscopist who was familiar with magnifying NBI. Hirata et al.[58] reported that microvascular features such as thickness and irregularity are associated with the histologic grade as well as with the depth of submucosal invasion. However, the image assessment method that they used is unclear.

Conclusions

NBI is a promising endoscopic technology that may improve detection and diagnostic accuracy for precancerous lesions and early cancer in the head and neck region, esophagus, stomach, duodenum, and colon. To date, many positive clinical data have been published. This brand-new technology enables us to detect early cancer or premalignant lesions in the GI tract, which will enable minimally invasive treatment or intensive surveillance of the patients.

However, most studies were conducted at a single institute and performed by a one or a few observers.

Table 5. Comparison of adenoma detection ability between conventional colonoscopy and NBI

Year	First author	Evaluation methods	*n* (patients)	Endoscopy system	Magnification	Modality	Results	*P* value	Ref. No
							Percentage of patients with >1 adenoma (all sizes)		
2007	Rex	Prospective RCT (WLI vs. NBI)	434	Color CCD chip system	–	WLI	67%	NS	46
						NBI	65%		
							Adenoma per patient, mean ± SD		
2007	Adler	Prospective RCT (WLI vs. NBI)	401	Color CCD chip system	–	WLI	0.26 (0.66)	NS	47
						NBI	0.33 (0.73)		
							Percentage of patients with >1 adenoma (>5 mm)		
2007	East	Back-to-back (WLI followed by NBI)	62	RGB sequential illumination system	+	WLI	27%	0.004	51
						NBI	42%		
							Percentage of patients with >1 adenoma (>5 mm)		
2008	Inoue	Prospective RCT (WLI vs. NBI)	243	RGB sequential illumination system	+/–	WLI	17%	0.011	52
						NBI	30%		
							Number of detected adenomas		
2008	Rastogi	Back-to-back after polypectomy (WLI followed by NBI)	40	Color CCD chip system	–	WLI	43		48
						NBI	29 additional adenomas		

RCT, randomized controlled trial

Then, we should confirm these data by a large-scale prospective randomized trial to standardize the diagnostic criteria.

References

1. Gono K, Yamazaki K, Doguchi N, Nonami T, Obi T, Yamaguchi M, et al. Endoscopic observation of tissue by narrow band illumination. Opt Rev 2003;10:1–5.
2. Gono K, Obi T, Yamaguchi M, Ohyama N, Machida H, Sano Y, et al. Appearance of enhanced tissue feature in narrow-band endoscopic imaging. J Biomed Opt 2004;9:568–77.
3. Muto M, Katada C, Sano Y, Yoshida S. Narrowband imaging: a new diagnostic approach to visualize angiogenesis in the superficial neoplasm. Clin Gastroenterol Hepatol 2005;3:S16–20.
4. Muto M, Ugumori T, Sano Y, Ohtsu A, Yoshida S. Narrow band imaging combined with magnified endoscopy for the cancer at the head and neck region. Dig Endosc 2005;17:S23–4.
5. Machida H, Sano Y, Hamamoto Y, Muto M, Kozu T, Tajiri H, et al. Narrow-band imaging in the diagnosis of colorectal lesions: a pilot study. Endoscopy 2004;36:1094–8.
6. Inoue H, Honda T, Nagai K, Kawano T, Yoshino K, Takeshita K, et al. Ultra-high magnification endoscopic observation of carcinoma in situ of the oesophagus. Dig Endosc 1997;9:16–8.
7. Kumagai Y, Inoue H, Nagai K, Kawano T, Iwai T. Magnifying endoscopy, stereoscopic microscopy, and the microvascular architecture of superficial esophageal carcinoma. Endoscopy 2002;34: 369–75.
8. Yao K, Oishi T. Microgastroscopic findings of mucosal microvascular architecture as visualized by magnifying endoscopy. Dig Endosc 2001;13:S27–33.
9. Yao K, Oishi T, Matsui T, Yao T, Iwashita A. Novel magnified endoscopic findings of microvascular architecture in intramucosal gastric cancer. Gastrointest Endosc 2002;56:279–84.
10. Sano Y, Kobayashi M, Hamamoto Y, Kato S, Fu KI, Yoshino T, et al. New diagnostic method based on color imaging using narrow-band imaging (NBI) system for gastrointestinal tract [abstract]. Gastrointest Endosc 2001;53:AB125.
11. Kaltenbach T, Sano Y, Friedland S, Soetikno R. American Gastroenterological Association (AGA) institute technology assessment on image-enhanced endoscopy. Gastroenterology 2008;134: 327–40.
12. Inoue H, Rey JF, Lightdale C. Lugol chromoendoscopy for esophageal squamous cell cancer. Endoscopy 2001;33:75–9.
13. Mori M, Adachi Y, Matsushima T, Matsuda H, Kuwano H, Sugimachi K. Lugol staining pattern and histology of esophageal lesions. Am J Gastroenterol 1993;88:701–5.
14. Yoshida T, Inoue H, Usui S, Satodate H, Fukami N, Kudo SE. Narrow-band imaging system with magnifying endoscopy for superficial esophageal lesions. Gastrointest Endosc 2004;59:288–9.
15. Muto M, Nakane M, Katada C, Sano Y, Ohtsu A, Esumi H, et al. Squamous cell carcinoma in situ at oropharyngeal and hypopharyngeal mucosal sites. Cancer 2004101:1375–81.
16. Watanabe A, Tsujie H, Taniguchi M, Hosokawa M, Fujita M, Sasaki S. Laryngoscopic detection of pharyngeal carcinoma in situ with narrowband imaging. Laryngoscope 2006;116:650–4.
17. Watanabe A, Taniguchi M, Tsujie H, Hosokawa M, Fujita M, Sasaki S. The value of narrow band imaging endoscope for early head and neck cancers. Otolaryngol Head Neck Surg 2008;138: 446–51.
18. Muto M, Saito Y, Ohmori T, Kaise M, Inoue H, Ishikawa H, et al. Multicenter prospective randomized controlled study on the detection and diagnosis of superficial squamous cell carcinoma by back-to-back endoscopic examination of narrowband imaging and white light observation. Gastrointest Endosc 2007;65:AB110.

19. Kiesslich R, Kanzler S, Vieth M, Moehler M, Neidig J, Thanka Nadar BJ, et al. Minimal change esophagitis: prospective comparison of endoscopic and histological markers between patients with non-erosive reflux disease and normal controls using magnifying endoscopy. Dig Dis 2004;22:221–7.
20. Sharma P, Wani S, Bansal A, Hall S, Puli S, Mathur S, et al. A feasibility trial of narrow band imaging endoscopy in patients with gastroesophageal reflux disease. Gastroenterology 2007;133:454–64.
21. Lee YC, Lin JT, Chie HM, Liao WC, Chen CC, Tu CH, et al. Intraobserver and interobserver consistency for grading esophagitis with narrow-band imaging. Gastrointest Endosc 2007;66: 230–6.
22. Hamamoto Y, Endo T, Nosho K, Arimura Y, Sato M, Imai K. Usefulness of narrow-band imaging endoscopy for diagnosis of Barrett's esophagus. J Gastroenterol 2004;39:14–20.
23. Kara MA, Peters FP, Rosmolen WD, Krishnadath KK, ten Kate FJ, Fockens P, et al. High-resolution endoscopy plus chromoendoscopy or narrow-band imaging in Barrett's esophagus: a prospective randomized crossover study. Endoscopy 2005;37:929–36.
24. Kara MA, Ennahachi M, Fockens P, ten Kate FJ, Bergman JJ. Detection and classification of the mucosal and vascular patterns (mucosal morphology) in Barrett's esophagus by using narrow band imaging. Gastrointest Endosc 2006;64:155–66.
25. Sharma P, Bansal A, Mathur S, Wani S, Cherian R, McGregor D, et al. The utility of a novel narrow band imaging endoscopy system in patients with Barrett's esophagus. Gastrointest Endosc 2006;64:167–75.
26. Goda K, Tajiri H, Ikegami M, Urashima M, Nakayoshi T, Kaise M. Usefulness of magnifying endoscopy with narrow band imaging for the detection of specialized intestinal metaplasia in columnar-lined esophagus and Barrett's adenocarcinoma. Gastrointest Endosc 2007;65:36–46.
27. Anagnostopoulos GK, Yao K, Kaye P, Hawkey CJ, Ragunath K. Novel endoscopic observation in Barrett's oesophagus using high resolution endoscopy and narrow band imaging. Aliment Pharmacol Ther 2007;26:501–7.
28. Singh R, Anagnostopoulos GK, Yao K, Karageorgiou H, Fortun PJ, Shonde A, et al. Narrow-band imaging with magnification in Barrett' esophagus: validation of simplified grading system of mucosal morphology pattern against histology. Endoscopy 2008; 40:457–63.
29. Curvers W, Baak L, Keisslich R, Van Oijen A, Rabenstein T, Ragunath K, et al. Chromoendoscopy and narrow band imaging compared with high-resolution magnification endoscopy in Barrett's esophagus. Gastroenterology 2008;134:670–9.
30. Wolfsen H, Crook JE, Krishna M, Achem SR, Devault KR, Bouras EP, et al. Prospective, controlled tandem endoscopy study of narrow band imaging for dysplasia detection in Barrett's esophagus. Gastroenterology 2008;135:24–31.
31. Uedo N, Ishihara R, Iishi H, Yamamoto S, Yamamoto S, Yamada T, et al. A new method of diagnosing gastric intestinal metaplasia: narrow band imaging with magnifying endoscopy. Endoscopy 2006;38:819–24.
32. Bansal A, Ulusarac O, Mathur S, Sharma P. Correlation between narrow band imaging and nonneoplastic gastric pathology: a pilot feasibility trial. Gastrointest Endosc 2008;67:210–6.
33. Yao K, Iwasita A, Tanabe H, Nagahama T, Matsui T, Ueki T, et al. Novel zoom endoscopy technique for diagnosis of small flat gastric cancer: a prospective, blind study. Clin Gastroenterol Hepatol 2007;5:869–78.
34. Nakayoshi T, Tajiri H, Matsuda K, Kaise M, Ikegami M, Sasaki H. Magnifying endoscopy combined with narrow band imaging system for early gastric cancer: correlation of vascular pattern with histopathology. Endoscopy 2004;36:1080–4.
35. Sumiyama K, Kaise M, Nakayoshi T, Kato M, Mashiko T, Uchiyama Y, et al. Combined use of a magnifying endoscope with a narrow band imaging system and a multibending endoscope for en bloc EMR of early stage gastric cancer. Gastrointest Endosc 2004;60:79–84.
36. Tamai N, Kaise M, Nakayoshi T, Katoh M, Sumiyama K, Gohda K, et al. Clinical and endoscopic characterization of depressed gastric adenoma. Endoscopy 2006;38:391–4.
37. Uchiyama Y, Imazu H, Kazutani H, Hino S, Sumiyama K, Kuramochi A, et al. New approach to diagnosing ampullary tumors by magnifying endoscopy with a narrow-band imaging system. J Gastroenterol 2006;41:483–90.
38. Vogelstein B, Fearon ER, Hamilton SR, Kern SE, Preisinger AC, Leppert M, et al. Genetic alterations during colorectal-tumor development. N Engl J Med 1988;319:525–32.
39. Vatan MH, Stalsbert H. The prevalence of polyps of large intestine in Oslo: an autopsy study. Cancer 1982;40:819–25.
40. Rex DK, Cutler CS, Lemmel GT, Rahmani EY, Clark DW, Helper DJ, et al. Colonoscopic miss rates of adenomas determined by back-to-back colonoscopies. Gastroenterology 1997; 112:24–8.
41. Van Rijn JC, Reitsma JB, Stoker J, Bossuyt PM, van Deventer SJ, Dekker E. Polyp miss rate determined by tandem colonoscopy: a systematic review. Am J Gastroenterol 2006;101:343–50.
42. Heresbach D, Barrioz T, Lapalus MG, Coumaros D, Bauret P, Potier P, et al. Miss rate for colorectal neoplastic polyps: a prospective multicenter study of back-to-back video colonoscopies. Endoscopy 2008;40:284–90.
43. Fu KI, Sano Y, Kato S, Fujii T, Nagashima F, Yoshino T, et al. Chromoendoscopy using indigo carmine dye spraying with magnifying observation is the most reliable method for differential diagnosis between non-neoplastic and neoplastic colorectal lesions: a prospective study. Endoscopy 2004;36:1089–93.
44. Su MY, Hsu CM, Ho YP, Chen PC, Lin CJ, Chiu CT. Comparative study of conventional colonoscopy, chromoendoscopy, and narrow-band imaging systems in differential diagnosis of neoplastic and nonneoplastic colonic polyps. Am J Gastroenterol 2006; 101:2711–6.
45. Chiu HM, Chang CY, Chen CC, Lee YC, Wu MS, Lin JT, et al. A prospective comparative study of narrowband imaging, chromoendoscopy, and conventional colonoscopy in the diagnosis of colorectal neoplasia. Gut 2007;56:373–9.
46. Rex DK, Helbig CC. High yields of small and flat adenomas with high-definition colonoscopes using either white light or narrow band imaging. Gastroenterology 2007;133:42–7.
47. Adler A, Pohl H, Papanikolaou IS, Abou-Rebyeh H, Schachschal G, Veltzke-Schlieker W, et al. A prospective randomized study on narrow-band imaging versus conventional colonoscopy for adenoma detection: does NBI induce a learning effect? Gut 2008; 57:59–64.
48. Rastogi A, Bansal A, Wani S, Callahan P, McGregor DH, Cherian R, et al. Narrow-band imaging colonoscopy—a pilot feasibility study for the detection of polyps and correlation of surface patterns with polyp histologic diagnosis. Gastrointest Endosc 2008; 67:280–6.
49. Jarvinen HJ, Mecklin JP, Sistonen P. Screening reduces colorectal cancer rate in families with hereditary nonpolyposis colorectal cancer. Gastroenterology 1995;108:1405–11.
50. Jarvinen HJ, Aarnio M, Mustonen H, Aktan-Collan K, Aaltonen LA, Peltomäki P, et al. Controlled 15-year trial on screening for colorectal cancer in families with hereditary nonpolyposis colorectal cancer. Gastroenterology 2000;118:829–34.
51. East JE, Suzuki N, Stavrinidis M, Guenther T, Thomas HJW, Saunders BP. Narrow band imaging for colonoscopic surveillance in hereditary nonpolyposis colorectal cancer. Gut 2008;57:65–70.
52. Inoue T, Murano M, Murano N, Kuramoto T, Kawakami K, Abe Y, et al. Comparative study of conventional colonoscopy and pan-colonic narrow-band imaging system in the detection of neoplastic colonic polyps: a randomized, controlled trial. J Gastroenterol 2008;43:45–50.
53. Uraoka T, Saito Y, Matsuda T, Sano Y, Ikehara H, Mashimo Y, et al. Detectability of colorectal neoplastic lesions using a narrow-

band imaging system: a pilot study. J Gastroenterol Hepatol (in press).
54. Kudo S, Hirota S, Nakajima T, Hosobe S, Kusaka H, Kobayashi T, et al. Colorectal tumours and pit pattern. J Clin Pathol 1994;47:880–5.
55. East JE, Suzuki N, Saunders BP. Comparison of magnified pit pattern interpretation with narrow band imaging versus chromoendoscopy for diminutive colonic polyps: a pilot study. Gastrointest Endosc 2007;66:310–6.
56. Hirata M, Tanaka S, Oka S, Kaneko I, Yoshida S, Yoshihara M, et al. Magnifying endoscopy with narrow band imaging for diagnosis of colorectal tumors. Gastrointest Endosc 2007;65:988–95.
57. Katagiri A, Fu KI, Sano Y, Ikematsu H, Horimatsu T, Kaneko K, et al. Narrow band imaging with magnifying colonoscopy as a diagnostic tool for predicting the histology of early colorectal neoplasia. Aliment Pharmacol Ther 2008;27:1269–74.
58. Hirata M, Tanaka S, Oka S, Kaneko I, Yoshida S, Yoshihara M, et al. Evaluation of microvessels in colorectal tumors by narrow band imaging magnification. Gastrointest Endosc 2007;66: 945–52.

Research Article

Pituitary Tumor-Transforming 1 Increases Cell Motility and Promotes Lymph Node Metastasis in Esophageal Squamous Cell Carcinoma

Tetsuo Ito,[1,2] Yutaka Shimada,[4] Takatsugu Kan,[1] Stefan David,[1] Yulan Cheng,[1] Yuriko Mori,[1] Rachana Agarwal,[1] Bogdan Paun,[1] Zhe Jin,[1] Alexandru Olaru,[1] James P. Hamilton,[1] Jian Yang,[1] John M. Abraham,[1] Stephen J. Meltzer,[1] and Fumiaki Sato[1,3]

[1]Division of Gastroenterology, Department of Medicine, and Sidney Kimmel Comprehensive Cancer Center, Johns Hopkins University School of Medicine, Baltimore, Maryland; [2]Department of Surgery, Graduate School of Medicine, and [3]Department of Nanobio Drug Discovery, Graduate School of Pharmaceutical Sciences, Kyoto University, Kyoto, Japan; and [4]Department of Surgery and Science, Graduate School of Medicine and Pharmaceutical Sciences Research, University of Toyama, Toyama, Japan

Abstract

Human pituitary tumor-transforming 1 (PTTG1)/securin is a putative oncoprotein that is overexpressed in various tumor types. However, the involvement of PTTG1 in gastrointestinal cancer development and progression remains unclear. In this study, we investigated the clinical significance and biological effects of PTTG1 in esophageal squamous cell carcinoma (ESCC). Immunohistochemical studies performed on 113 primary ESCC specimens revealed a high prevalence of PTTG1 overexpression (60.2%), which was significantly associated with lymph node metastasis (regional, $P = 0.042$; distant, $P = 0.005$), advanced tumor stage ($P = 0.028$), and poorer overall survival ($P = 0.017$, log-rank test; $P = 0.044$, Cox proportional hazard model). Eleven ESCC cell lines expressed PTTG1 protein at levels 2.4 to 6.6 times higher than those in normal esophageal epithelial cells (HEEpiC). PTTG1 protein expression was confined to the nucleus in HEEpiC cells but present in both the cytoplasm and nucleus in ESCC cells. Two small interfering RNAs (siRNA) inhibited PTTG1 mRNA and protein expression in three ESCC cell lines by 77% to 97%. In addition, PTTG1 down-regulation by these siRNAs significantly reduced cell motility in all three ESCC cell lines ($P < 0.01$) *in vitro*, as well as popliteal lymph node metastases of ESCC cells in nude mice ($P = 0.020$). Global gene expression profiling suggested that several members of the Ras and Rho gene families, including *RRAS*, *RHOG*, *ARHGAP1*, and *ARHGADIA*, represented potential downstream genes in the PTTG1 pathway. Taken together, these findings suggest that PTTG1 overexpression promotes cell motility and lymph node metastasis in ESCC patients, leading to poorer survival. Thus, PTTG1 constitutes a potential biomarker and therapeutic target in ESCCs with lymph node metastases. [Cancer Res 2008;68(9):3214–24]

Introduction

Esophageal squamous cell carcinoma (ESCC) is a highly aggressive malignancy with a 5-year survival rate of 10% worldwide (1). One reason for this poor survival is the fact that ESCC frequently metastasizes to regional and distant lymph nodes, even at initial diagnosis. Lymph node metastasis is one of the most important prognostic factors in ESCC (2). Therefore, the detection and treatment of lymph node metastases are extremely important in managing this refractory cancer.

Pituitary tumor-transforming 1 (PTTG1), also known as human securin, was originally isolated from rat pituitary tumor cells (3). PTTG1 possesses multiple physiologic functions critical to normal cellular mitosis, which are exerted through the maintenance of sister chromatid separation (4). PTTG1 overexpression has been reported in a variety of cancers including ESCC (5–7). PTTG1 levels correlate with tumor invasiveness (8), and PTTG1 has been identified as a key signature gene in tumor metastasis (9). However, mechanisms underlying the involvement of PTTG1 in lymph node metastasis are poorly understood.

Recently, we discovered that *PTTG1* was overexpressed in ESCC tumors versus normal organs and exhibited much higher promoter activity in ESCC cells than in normal epithelial cells (10). Based on these findings, we hypothesized that PTTG1 represented a promising potential therapeutic target in ESCC. Nevertheless, the clinical significance and biological involvement of PTTG1 in the progression of gastrointestinal cancers, including ESCCs, have not yet been elucidated. Therefore, we sought to clarify the clinical effect and the *in vitro* and *in vivo* biological functions of PTTG1 in ESCC, using 113 surgically resected primary ESCC specimens, small interfering RNAs (siRNA) directed against PTTG1, esophageal cell lines, and *in vitro* and *in vivo* metastasis assays.

Materials and Methods

Patients and surgical specimens. Paraffin-embedded sections were obtained for immunohistochemical studies from 113 patients with primary ESCC undergoing surgery at Kyoto University Hospital (Kyoto, Japan) from 1991 to 2002. The median age of these patients was 62.5 y (range, 43–82 y). Median postoperative survival was 80 mo (range, 1–159 mo). Information on gender, age, stage of disease, and histopathologic features was abstracted from medical records. All tumors were confirmed as ESCC by the Clinicopathologic Department at Kyoto University Hospital. All cases were classified according to the sixth edition of the pathologic tumor-node-metastasis (pTNM) classification (11). Written informed consent for the research use of resected specimens was obtained from all patients before

Note: Supplementary data for this article are available at Cancer Research Online (http://cancerres.aacrjournals.org/).

Requests for reprints: Fumiaki Sato, Department of Nanobio Drug Discovery, Graduate School of Pharmaceutical Sciences, Kyoto University, Main Building A320, Shimoadachi-cho 46-29, Yoshida, Sakyo-ku, Kyoto 606-8501, Japan. Phone: 81-75-753-9559; Fax: 81-75-753-9557; E-mail: fsato@pharm.kyoto-u.ac.jp, or Stephen J. Meltzer, Division of Gastroenterology, Department of Medicine, Johns Hopkins University School of Medicine, Room 112, 1503 East Jefferson Street, Baltimore, MD 21231. Phone: 410-502-6071; Fax: 410-502-1099; E-mail: smeltzer@jhmi.edu.

doi:10.1158/0008-5472.CAN-07-3043

Table 1. PTTG1 protein expression in 113 primary ESCC tumors determined by immunohistochemistry

(*A*) PTTG1 staining and clinicopathologic characteristics in 113 ESCC patients

Variables	PTTG1 (– or +), $n = 45$	PTTG1 (++ or +++), $n = 68$	*P*
Age, y			0.373
Mean	63.7	62.1	
SD	8.6	9.6	
Gender			0.679
Male	39	57	
Female	6	11	
pT (primary tumor)			0.933
pT_1	15	19	
pT_2	9	16	
pT_3	16	25	
pT_4	5	8	
pN (regional lymph node metastasis)			0.042*
pN_0	21	19	
pN_1	24	49	
pM (distant lymph node metastasis)			0.005*
pM_0	42	49	
pM_1	3	19	
pTNM stage			0.028*
I	12	11	
IIa	9	8	
IIb	6	15	
III	14	16	
IVa	0	9	
IVb	3	10	
Histologic grade			0.063
1	11	6	
2	24	40	
3	10	22	

(*B*) Cox univariate analysis

Variables	Risk ratio (95% CI)	*P*
Age (>63 y)	1.01 (0.61–1.68)	0.957
Gender (male)	1.36 (0.72–2.57)	0.337
pT (>T_1)	3.65 (2.13–6.26)	0.0001
pN (1)	3.48 (1.87–6.46)	0.0001
pM (1)	2.28 (1.28–4.06)	0.0051
Histologic grade (>G2)	1.28 (0.61–2.69)	0.52
PTTG1 (++ or +++)	1.75 (1.01–3.00)	0.044

(*C*) Cox multivariate analysis

Variables	Risk ratio (95% CI)	*P*
Age (>63 y)	1.08 (0.63–1.84)	0.784
Gender (male)	0.82 (0.43–1.66)	0.561
pT (>T_1)	2.91 (1.67–5.26)	0.0001
pN (1)	2.23 (1.16–4.54)	0.016
pM (1)	1.12 (0.58–2.12)	0.723
Histologic grade (>G2)	1.04 (0.49–2.50)	0.914
PTTG1 (++ or +++)	1.61 (0.92–2.91)	0.093

* Pearson's χ^2 test.

surgery; approval was obtained from the Kyoto University Institutional Review Board (nos. #232 and #G48).

Antibodies and siRNAs. Anti-human PTTG1 rabbit polyclonal antibody, clone Z23 (Invitrogen; diluted 1:250), was used for immunohistochemical studies, Western blotting, and immunofluorescence staining (diluted 1:200). Mouse monoclonal anti-human β-actin antibody, clone AC-15 (1:10,000; Sigma), mouse monoclonal anti-lamin A/C antibody (1:100; Santa Cruz Biotechnology), and mouse monoclonal anti-glyceraldehyde-3-

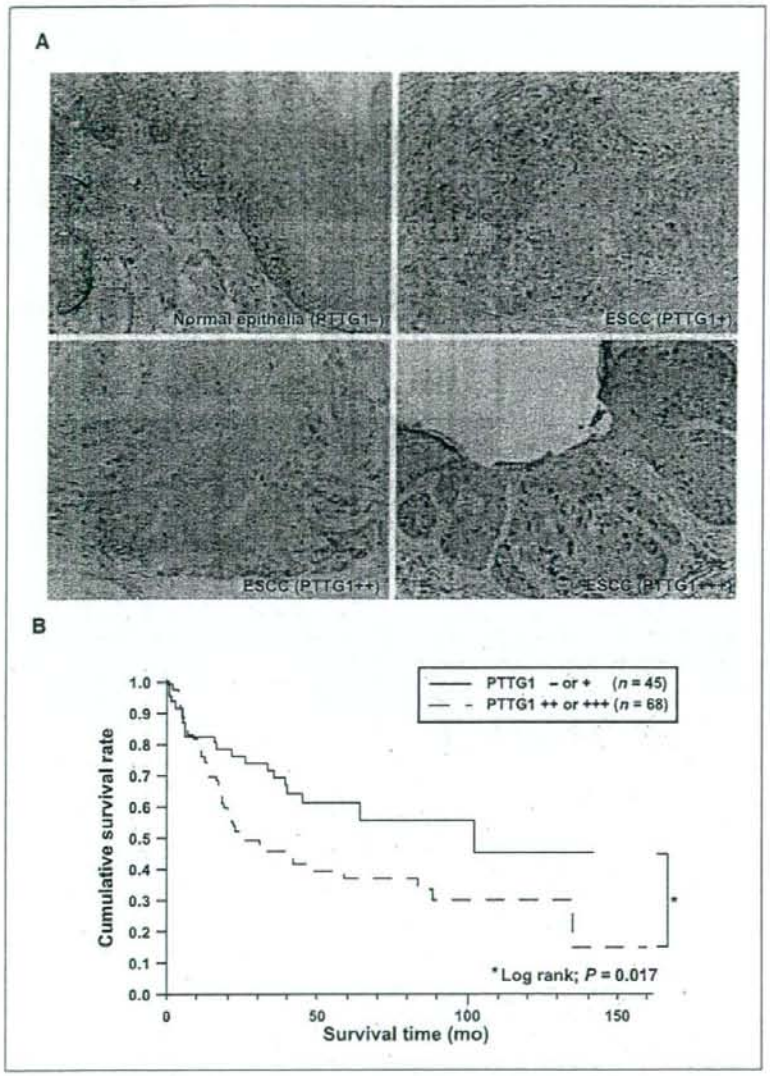

Figure 1. PTTG1 protein expression in ESCC tumor tissues and cell lines. *A*, PTTG1 protein expression level in primary ESCC tumors was classified according to cytoplasmic staining of PTTG1. *Top left*, normal esophageal epithelium with negative PTTG1 expression; *top right*, ESCC with weak PTTG1 expression (1+, 0–10% of cells stained); *bottom left*, ESCC with moderate PTTG1 expression (2+, 10–30%); *bottom right*, ESCC with strong PTTG1 expression (3+, >30%). *B*, overall survival analysis by the Kaplan-Meier method. Primary ESCCs with moderate to strong PTTG1 expression (2+ and 3+) were classified as PTTG1 positive. Patients with PTTG1-positive tumors ($n = 68$) had significantly worse survival than did those with PTTG1-negative tumors ($n = 45$; $P = 0.017$, log-rank test).

phosphate (GAPDH) antibody, clone 71.1 (1:20,000; Sigma), were used for Western blotting. Horseradish peroxidase–labeled antirabbit IgG (1:2,500; Chemicon) or antimouse IgG (1:5,000; Invitrogen) was used as a secondary antibody for Western blotting. Two siRNAs directed against PTTG1 (P1 and P2) were synthesized by Dharmacon. P1 was designed by the authors via siDirect, an siRNA design software (12), whereas P2 had previously been designed by others (13). The siRNA target sequences were as follows: P1, 5′-GTGACATAGATATTTAAAT-3′ (position 638–656, NM_004219); P2, 5′-GTCTGTAAAGACCAAGGGA-3′ (position 264–282). A nontargeting control siRNA (NTC; Dharmacon) served as a negative control.

Immunohistochemical staining. Resected esophageal specimens were fixed in 10% formaldehyde and embedded in paraffin blocks. Using 4-μm-thick sections, immunohistochemical staining was done with an Envision kit (DakoCytomation; ref. 14). As a negative control, the primary antibody was replaced with a normal mouse IgG. All slides were independently evaluated by two investigators (T.I. and Y.S.) lacking prior knowledge of each patient's clinical information. Whenever opinions of these two evaluators differed, agreement was reached by careful discussion.

Cell cultures. Human ESCC cell lines of the KYSE series, as well as HSA/c, were established and maintained in Ham's F12/RPMI 1640 (Invitrogen) containing 5% fetal bovine serum (FBS), as previously described (14, 15). Nonmalignant human esophageal epithelial cells (HEEpiC; ScienCell) were maintained in Epithelial Cell Medium 2 (ScienCell) according to the provider's instructions.

Western blotting and subcellular fractionation. Cells were washed with PBS and lysed in Laemmli sample buffer (Bio-Rad) at room temperature. Protein concentration was estimated with BCA Protein Assay kit (Pierce). Cell lysates (15 μg) were electrophoresed on a 15% polyacrylamide gel (Bio-Rad) and transferred onto polyvinylidene difluoride

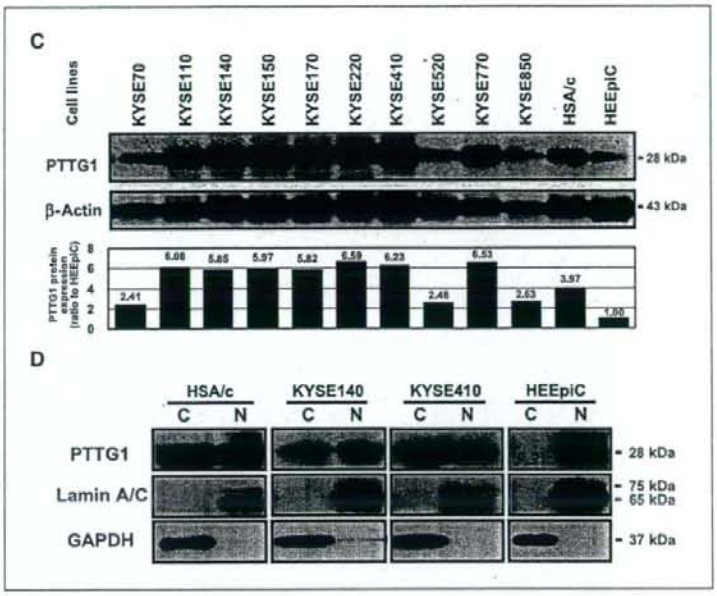

Figure 1 *Continued*. *C*, PTTG1 protein expression in 11 ESCC cell lines and in primary-cultured normal esophageal epithelial cells (HEEpiC). Equal amounts of whole cellular protein (15 μg) were loaded in all lanes. Immunoblot membranes were probed with anti-PTTG1 or anti–β-actin antibodies. The KYSE series and HSA/c composed the human ESCC cell lines. *Bottom*, PTTG1 expression fold change in ESCC cell lines relative to HEEpiC, normalized to β-actin expression. *D*, subcellular localization of PTTG1 in ESCC cell lines (HSA/c, KYSE140, and KYSE410) and HEEpiC. Equal amounts of the cytoplasmic or nuclear fractionated protein (20 μg) were loaded in all lanes. Purity of fractions was verified with anti-GAPDH (cytoplasm) and anti–lamin A/C (nucleus) antibodies. *C*, cytoplasmic fraction; *N*, nuclear fraction.

membranes (Millipore). After being blocked with TBS containing 5% skim milk and 0.1% Tween 20 for 1 h, membranes were incubated with the primary and secondary antibodies at room temperature for 2 and 1 h, respectively, and then bands were visualized with enhanced chemiluminescence plus reagent (GE Healthcare). All bands were quantified using ImageJ v1.34 (U.S. NIH).[5] For subcellular fractionation assays, nuclear and cytoplasmic fractions were separated with NE-PER Nuclear and Cytoplasmic Extraction Reagents (Pierce). GAPDH and lamin A/C were used as cytoplasmic and nuclear markers, respectively, as previously described (16, 17).

Transfections. Three ESCC cell lines (i.e., KYSE140, KYSE410, and HSA/c) were separately and transiently transfected with three siRNAs, specifically NTC, P1, and P2, using Lipofectamine RNAiMAX (LF; Invitrogen) according to the manufacturer's protocol. Cells were plated at 2×10^5 per well onto six-well plates (Corning) 1 d before transfection (day 0). The siRNA (200 pmol/well) was transfected into cells at day 1, and total RNA and protein were extracted at day 4. No treatment (LF−) and Lipofectamine RNAiMAX alone (LF+) were included as negative controls.

Quantitative reverse transcription-PCR analysis. Total RNA was extracted with Trizol reagent (Invitrogen). Quantitative reverse transcription-PCR (RT-PCR) with SYBR Green QuantiTect RT-PCR kit (Qiagen) was done on an iQ5 real-time PCR machine (Bio-Rad) as previously described (10). mRNA expression in each sample was normalized to average β-actin expression in each sample. The primer sequences are listed in Supplementary Table S1.

Immunofluorescence staining. Immunofluorescence staining was done as previously described (18). Briefly, siRNA-transfected cells were seeded onto a coverslip at day 4 and incubated for 1 additional day. Cells were fixed with 1% formaldehyde in PBS for 15 min, treated with 0.2% Triton X-100 in PBS for 10 min, blocked with 1% bovine serum albumin in PBS, and incubated with a primary antibody and antirabbit Alexa Fluor 568 (Invitrogen) at room temperature for 1 h and 30 min, respectively. Nuclei were counterstained with 4′,6-diamidino-2-phenylindole (DAPI; Roche Diagnostics). The cells were mounted and viewed under a fluorescence microscope (Carl Zeiss).

Cell migration/invasion assays. Cell motility (chemotaxis) and invasiveness were determined with Transwell and Matrigel chamber inserts, respectively (24-well-format with 8-μm pores, BD Biosciences), as previously described (19). Cells (5×10^4) were seeded onto the upper chamber at day 4, with 20% FBS in the lower chamber as a chemoattractant. After incubation at 37°C for 24 h, membranes were stained and all cells on the lower membrane surface were counted under a light microscope. The number of cells migrating through Matrigel inserts represented a combination of cell penetration through the Matrigel layer and cell migration through the small membrane pores (20). To distinguish between these two biological processes, we defined an invasion index (i.e., cell penetration through the Matrigel layer) as the ratio of the mean number of cells migrating through the Matrigel insert to the mean number of cells migrating through the Transwell membrane.

***In vivo* lymph node metastasis assay.** This assay was done using an *in vivo* popliteal lymph node metastasis model (14). HSA/c cells (3×10^6) were transfected with an siRNA *in vitro*, harvested 72 h after transfection, and inoculated into both footpads of 5-wk-old male athymic nude mice (Harlan) at day 0. SiRNA (20 μg) conjugated with polyethylenimine (*in vivo* jetPEI, Polyplus Transfection) was injected intratumorally on days 7, 14, and 21. Polyethylenimine/siRNA complexes were prepared at a polyethylenimine/siRNA (N/P) ratio equal to 10, as previously described (21). For vehicle control treatments, Lipofectamine RNAiMAX (Invitrogen) and polyethylenimine (Polyplus Transfection) without siRNA were used *in vitro* and *in vivo*, respectively. Ten primary footpad tumors from five mice were analyzed for each treatment condition (vehicle, NTC, P1, and P2). All mice were sacrificed at day 28, and all primary tumors and popliteal lymph nodes were enucleated and fixed in 10% formaldehyde/PBS. All lymph nodes and primary tumors were paraffin embedded, stained with H&E and PTTG1, and examined for the presence of metastases. All animal procedures were approved by the institutional animal committee and executed in accordance with institutional guidelines.

Bead-array gene expression analyses. HSA/c and KYSE140 cells were separately transfected with one of three siRNAs (NTC, P1, and P2) or with

5 Available at http://rsb.info.nih.gov/ij/index.html.

Lipofectamine alone (LF+), as described above, and harvested 72 h after transfection. Following RNA quality assessment done on a Bioanalyzer 2100 (Agilent Technologies), each RNA sample (100 ng), extracted using an RNeasy kit (Qiagen), was amplified with an Illumina TotalPrep RNA Amplification kit (Ambion), hybridized to an Illumina Human RefSeq8 version 2 BeadChip containing 20,589 transcript probes composed of optimized 50-mer oligonucleotides (Illumina), washed, and stained with Cy3-streptavidin (GE Healthcare) per manufacturer's instructions (22). Arrays were scanned with Illumina Beadarray Reader confocal scanner and data were processed using Illumina BeadStudio software. Data were subjected to intensity-dependent normalization, and differentially expressed genes associated with PTTG1 down-regulation

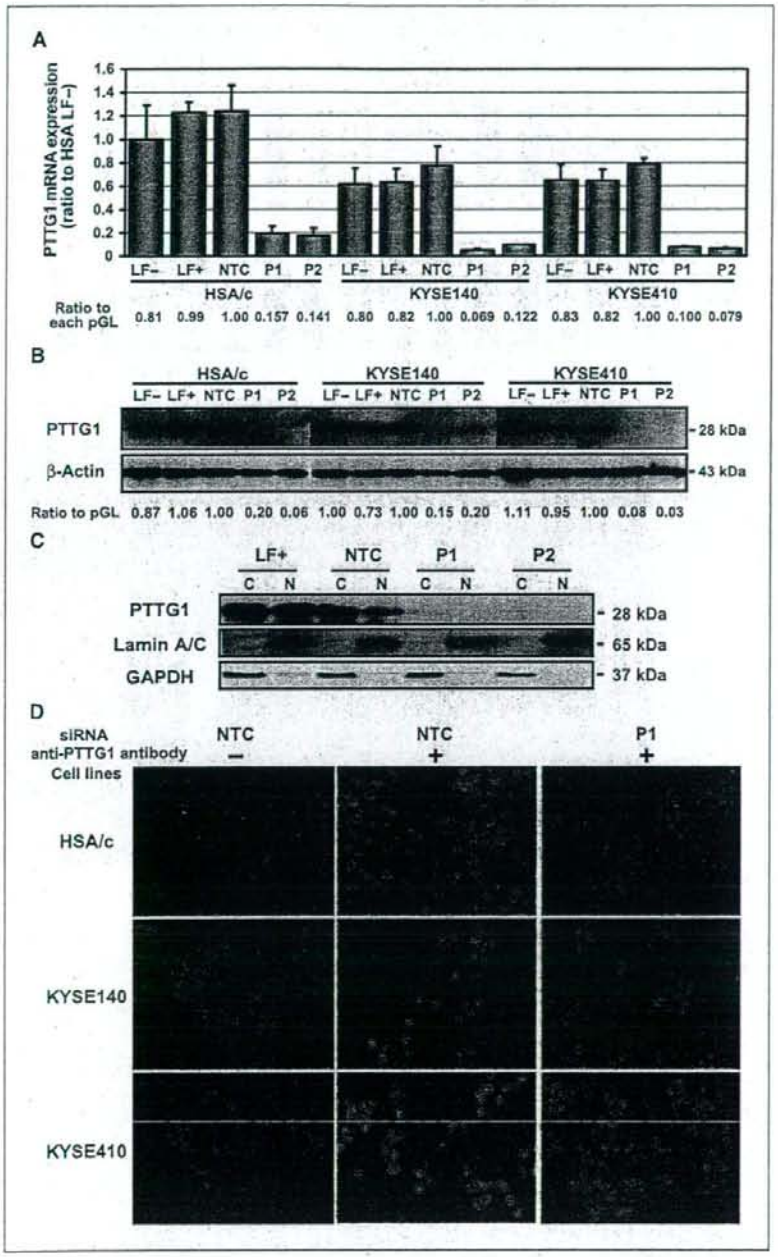

Figure 2. Knockdown of PTTG1 expression in ESCC cells by siRNAs. HSA/c, KYSE140, and KYSE410 cells were transfected using the following conditions: LF−, untransfected control; LF+, transfection with Lipofectamine RNAiMAX alone; NTC, nontargeting control siRNA; P1, siRNA 1 directed against PTTG1; P2, siRNA 2 directed against PTTG1. *A*, PTTG1 mRNA expression levels in siRNA-treated cells. Each value represents the ratio of PTTG1 level versus HSA/c LF−, normalized to β-actin. Numbers at the bottom represent the ratio of PTTG1 expression for each condition relative to NTC-transfected cells. *B*, PTTG1 protein expression in siRNA-treated cells. Equal amounts of whole cellular protein (9 μg) were loaded in all lanes. Numbers at the bottom represent the ratio of PTTG1 expression for each condition relative to PTTG1 expression in NTC-transfected cells. *C*, subcellular localization of PTTG1 in siRNA-treated HSA/c cells. Equal amounts of cytoplasmic or nuclear fractionated protein (20 μg) were loaded in all lanes. Purity of fractions was verified with anti-GAPDH (cytoplasm) and anti–lamin A/C (nucleus) antibodies. *D*, immunofluorescence staining for PTTG1. Cells were stained with PTTG1, which was labeled with Alexa Fluor 568 (*red*), and nuclei were counterstained with DAPI (*blue*). *Left*, cells transfected with NTC stained without PTTG1 primary antibody and only with secondary antibody-Alexa Fluor 568; *middle*, cells transfected with NTC; *right*, cells transfected with P1. Photographs were taken at identical exposure intervals (18.2 ms; magnification, ×100).

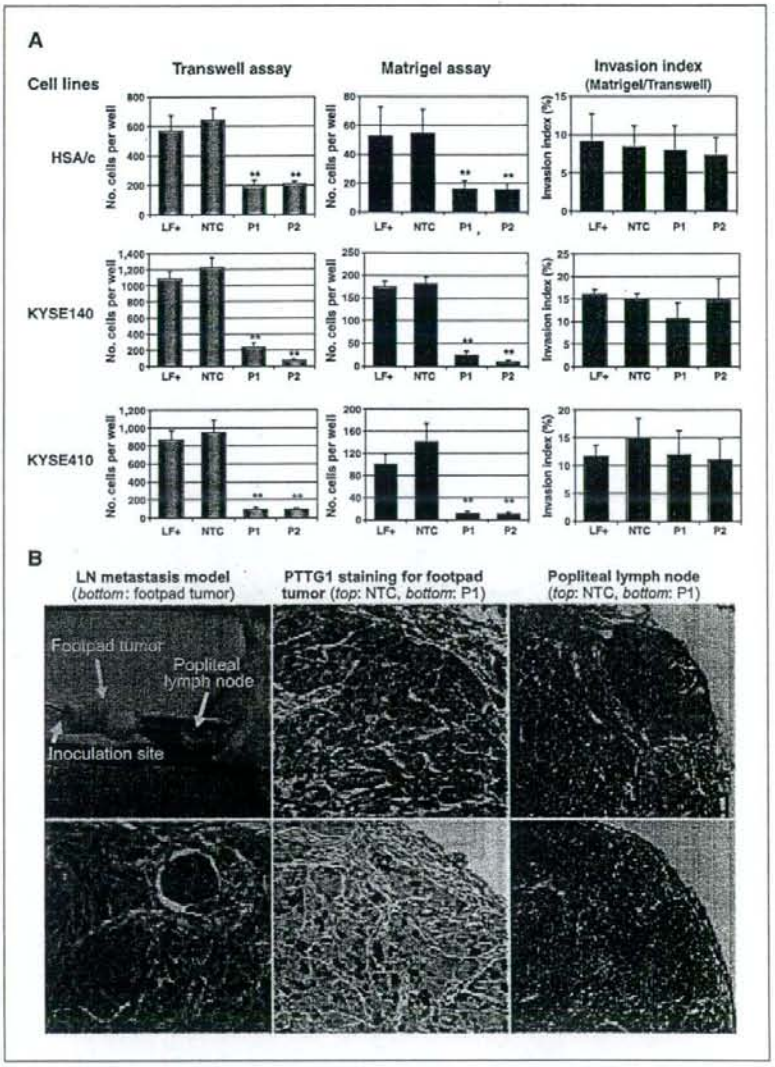

Figure 3. Effects of PTTG1 knockdown on cell migration *in vitro* and lymph node metastasis *in vivo*. *A*, cell migration/invasion assays *in vitro*. *Columns*, mean of triplicate experiments; *bars*, SD. *Left*, Transwell migration assay; numbers of cells migrating through Transwell membranes are shown. *Middle*, Matrigel invasion assay; numbers of cells migrating through Matrigel inserts are shown. *Right*, invasion index (%); ratios of cells migrating through Matrigel inserts relative to mean numbers of cells migrating through Transwell membranes are shown. **, $P < 0.01$, versus NTC for each group (Tukey-Kramer test). *B*, lymph node metastasis assay in nude mice. *Top left*, a leg of a nude mouse at 28 d after inoculation of HSA/c cells into the footpad. The leg skin was stripped to show a swollen popliteal lymph node. The distance between the footpad tumor and the popliteal lymph node was ~1 cm. *Bottom left*, H&E staining of a footpad tumor (magnification, ×200). Note the "cancer pearl" in the center. *Middle*, PTTG1 immunostaining of a footpad tumor treated with NTC (*top*) and P1 (*bottom*; magnification, ×100). *Right*, representative H&E staining of popliteal lymph nodes treated with NTC (*top*) and P1 (*bottom*; magnification, ×100).

were identified by significance analysis of microarrays (23). All processed and raw data are available in Minimum Information about Microarray Gene Experiment–compliant format via the Gene Expression Omnibus.[6] Accession numbers are GSE7447, GSM180360, GSM180361, GSM180362, GSM180363, GSM180364, GSM180365, GSM180366, GSM180367, and GSM180368. Expression profiles of HSA-P1, HSA-P2, KYSE140-P1, and KYSE140-P2, which were designated gene profiles associated with PTTG1 down-regulation, were compared with expression profiles of HSA-LF+, HSA-NTC, KYSE140-LF+, and KYSE140-NTC, which were considered intact-PTTG1 cell profiles. Fold changes on bead array were calculated by dividing the average signal intensity of all down-regulated-PTTG1 profiles by the average of all intact-PTTG1 profiles. For validation of expression profiles, the mRNA expression level of each gene was analyzed by quantitative RT-PCR, as described above. Fold change for each gene assessed by quantitative RT-PCR was calculated as the ratio of average expression in all PTTG1-downregulated cells (HSA-P1, HSA-P2, KYSE140-P1, and KYSE140-P2) to average expression in all intact-PTTG1 cells (HSA-LF+, HSA-NTC, KYSE140-LF+, and KYSE140-NTC). ELISA for basic fibroblast growth factor (bFGF; immunoassay kit, BioSource) was done with cell culture medium according to the manufacturer's protocol.

Statistical analyses. Survival curves were generated according to the Kaplan-Meier method, and differences in survival were analyzed by log-rank testing. Univariate and multivariate analyses were done using the Cox proportional hazards model. Correlations between PTTG1 expression and each clinicopathologic parameter were evaluated using Pearson's χ^2 test. The Tukey-Kramer multiple comparison test was used to evaluate

[6] http://www.ncbi.nlm.nih.gov/geo

Table 2. Effect of PTTG1 knockdown on lymph node metastasis *in vivo*

(*A*) PTTG1 siRNA treatment in lymph node metastasis model

Treatment	No. mice	No. total LNs	No. metastatic LNs	Metastatic ratio (%)
Vehicle	5	10	5	50
NTC	5	10	5	50
P1	5	10	2	20
P2	5	11	1	9.1
total	20	41	13	31.7

(*B*) Relationship between PTTG1 down-regulation and lymph node metastasis

PTTG1 status	No. metastatic LNs (%)	No. nonmetastatic LNs (%)
PTTG1(+)*	10 (50)	10 (50)
PTTG1(−)†	3 (14.3)	18 (85.7)
total	13 (31.7)	28 (68.3)

NOTE: Metastatic ratio = number of metastatic lymph nodes / number of total lymph nodes.
Abbreviation: LNs, lymph nodes.
* Vehicle and NTC (n = 20).
† P1 and P2 (n = 21); P = 0.020, Fisher's exact test.

phenotypes of each cell. All statistical calculations were done using StatView version 5 (SAS Institute) and Statistica version 6.1 (StatSoft). $P < 0.05$ was considered significant.

Results

PTTG1 protein expression in 113 primary ESCC tumors. As shown in Table 1*A*, 23 patients were with stage I, 17 with stage IIa, 21 with stage IIb, 30 with stage III, 9 with stage IVa, and 13 with stage IVb ESCCs. The pattern of PTTG1 staining in ESCC was different from that observed in normal epithelium. In ESCC cells, PTTG1 staining was usually observed in the cytoplasm and only occasionally in the nucleus (Fig. 1*A*). In contrast, PTTG1 staining in normal esophageal epithelia was never observed in the cytoplasm, but still occasionally in the nucleus (~10% of cases; data not shown), particularly in the proliferative layer just above the basal cells. PTTG1 expression in ESCC specimens, evaluated based exclusively on cytoplasmic staining, occurred as follows: 14 tumors were negative for expression (−), 31 manifested expression in 0% to 10% of tumor cells (1+), 52 revealed expression in 10% to 30% of tumor cells (2+), and 16 were characterized by expression in >30% of tumor cells (3+). Next, we classified 2+ or 3+ PTTG1 expression as PTTG1 positive (68 of 113, 60.2%). Under this classification system, PTTG1 expression was significantly associated with regional lymph node metastasis (pN; P = 0.042), distant lymph node metastasis (pM; P = 0.005), and tumor stage (pTNM; P = 0.028), but not with depth of primary tumor invasion (pT; P = 0.933). Kaplan-Meier survival analysis showed that patients with PTTG1-positive tumors had significantly worse survivals than did those with PTTG1-negative tumors (P = 0.017, log-rank test; Fig. 1*B*). Furthermore, univariate analyses revealed that PTTG1 expression was a significant predictor of survival [risk ratio, 1.75; 95% confidence interval (95% CI), 1.01–3.00; P = 0.044; Table 1*B*]. Multivariate analyses revealed that PTTG1 expression tended to be an independent prognostic factor, although this trend did not achieve statistical significance (risk ratio, 1.61; 95% CI, 0.92–2.91; P = 0.093; Table 1*C*). Several tumors showed strong PTTG protein expression in cell nuclei. We also evaluated nuclear staining in all 113 ESCC tumors. Nuclear PTTG1 protein expression occurring in >10% of tumor cells was observed in only 7 of 113 (6.2%) ESCC tumors. However, nuclear PTTG1 staining did not correlate with any clinicopathologic features or survival. We also compared the no-expression group (−; n = 14) to the any-expression group (1+–3+; n = 99). In this analysis, any level of PTTG1 expression was associated with distant lymph node metastasis (pM; P = 0.049), but not with primary tumor invasion (pT; P = 0.532), regional lymph node metastasis (pN; P = 0.222), tumor stage (pTNM; P = 0.523), or histologic grade (P = 0.098). Kaplan-Meier survival analysis showed a trend toward association of any PTTG1 expression with poor survival (P = 0.164, log-rank test). Interestingly, none of the 14 PTTG1-negative tumors gave rise to distant lymph node metastases.

PTTG1 protein expression in squamous esophageal cells. We performed Western blotting to assess PTTG1 protein levels in 11 ESCC cell lines and in cultured normal esophageal epithelial cells (HEEpiC; Fig. 1*C*). PTTG1 expression in all 11 ESCC cell lines was 2.4 to 6.6 times higher than in HEEpiC cells. To determine subcellular localization of PTTG1 expression, the relative nuclear versus cytoplasmic distribution of PTTG1 protein was examined in HSA/c, KYSE140, KYSE410, and HEEpiC cells by subcellular fractionation (Fig. 1*D*). Purity of fractions was verified by probing membranes with cytoplasmic (GAPDH) or nuclear (lamin A/C) protein-specific antibodies. PTTG1 in HEEpiC cells was expressed only in the nucleus, but not in the cytoplasm. Conversely, PTTG1 in HSA/c, KYSE140, and KYSE410 cells was expressed in both the cytoplasm and nucleus. To evaluate the effect of PTTG1 knockdown in ESCC cells, we selected HSA/c, KYSE140, and KYSE410 for further analyses because of their high native PTTG1 expression levels.

Knockdown of PTTG1 expression in ESCC cells. We transiently transfected either a PTTG1 siRNA (P1 or P2) or a

NTC into three different ESCC cell lines (HSA/c, KYSE140, and KYSE410). By quantitative RT-PCR, PTTG1 mRNA expression was inhibited by 84% to 86% in HSA/c, 88% to 93% in KYSE140, and 90% to 92% in KYSE410 cells (Fig. 2*A*). By Western blotting, PTTG1 protein expression was inhibited by 77% to 93% in HSA/c, 86% to 88% in KYSE140, and 92% to 97% in KYSE410 cells (Fig. 2*B*). By fluorescence microscopy and flow cytometry, we confirmed that transfected FAM-labeled siRNAs were taken up by >90% of cells (data not shown). A subcellular fractionation assay in PTTG1-down-regulated HSA/c cells showed that both of the PTTG1 siRNAs (P1 and P2) suppressed both nuclear and cytoplasmic PTTG1 expression (Fig. 2*C*). We also examined PTTG1 expression in these cells by immunofluorescence staining (Fig. 2*D*). Whereas PTTG1 was expressed in both the cytoplasm and nucleus of ESCC cells in negative control transfections (LF+ and NTC), the siRNAs directed against PTTG1 (P1 and P2) markedly suppressed PTTG1 expression in these cells, corroborating the results of Western blotting.

PTTG1 knockdown reduces motility of ESCC cells. Cell motility and invasiveness were determined by Transwell and Matrigel chamber assays, respectively (Fig. 3*A*). PTTG1 knockdown in HSA/c, KYSE140, and KYSE410 cells reduced the number of cells migrating through Transwell and Matrigel chambers by 94.0% to 67.8% and by 94.1% to 70.7%, respectively ($P < 0.01$, versus NTC). In contrast, invasion index, representing the degree of cell penetration through the Matrigel layer, was not altered by PTTG1 inhibition.

PTTG1 knockdown suppresses lymph node metastasis *in vivo*. We examined the effect of PTTG1 knockdown, using a popliteal lymph node metastasis model, in nude mice (Fig. 3*B*, *top left*). In separate experiments, highly metastatic HSA/c cells were transfected with either siRNA P1 or siRNA P2 and then inoculated into the footpads of nude mice at day 0. To maintain the knockdown effects of PTTG1, we carried out additional *in vivo* transfections by injecting siRNAs intratumorally with polyethylenimine weekly from day 7 to day 21. At day 28, all mice were sacrificed and all footpad tumors (Fig. 3*B*, *bottom left*) and popliteal lymph nodes were obtained and analyzed. PTTG1 immunostaining (Fig. 3*B*, *middle*) showed that PTTG1 expression in footpad tumors was inhibited by both PTTG1 siRNAs (P1 and P2) compared with negative control transfections (vehicle only and NTC). As shown in Table 2*A*, ratios of metastatic to total dissected popliteal lymph nodes were lower in both PTTG1 siRNA groups than in vehicle-only or NTC groups [50.0% (5 of 10) in vehicle, 50.0% (5 of 10) in NTC, 20.0% (2 of 10) in P1, and 9.1% (1 of 11) in P2]. Moreover, this difference in metastatic ratios achieved statistical significance ($P = 0.020$, Fisher's exact test; Table 2*B*) when metastatic ratios were compared between the PTTG1-down-regulated group [PTTG1(−): P1 and P2] and the intact-PTTG1 group [PTTG1(+): vehicle only and NTC]. Representative H&E staining of a metastatic lymph node in NTC and a nonmetastatic lymph node in P1 is shown in Fig. 3*B* (*top right* and *bottom right*, respectively).

Identification of potential downstream genes in the PTTG1 pathway in ESCC. To identify target genes potentially regulated by PTTG1, we conducted bead array–based genome-wide mRNA profiling. As shown in Table 3, PTTG1 siRNA treatment resulted in the up-regulation of 12 genes and down-regulation of 8 genes in HSA/c and KYSE140 cells. Differentially expressed genes previously reported as being cell motility–related included several Ras and Rho family members, such as *RRAS* (related-ras viral oncogene homologue), *RHOG* (ras homologue gene family, member G), *ARHGAP1* (Rho GTPase activating protein 1), and *ARHGDIA* (Rho GDP dissociation inhibitor α). We then confirmed differential expression of selected genes in these same RNA samples by quantitative RT-PCR and found that fold changes in gene expression discovered by bead array correlated strongly with fold changes found by quantitative RT-PCR ($r^2 = 0.885$; $P < 0.0001$, Pearson's correlation coefficient). *PTTG1* was identified as the gene most markedly down-regulated among 20,589 transcripts, closely agreeing with quantitative RT-PCR results for *PTTG1* (bead-array fold change, 0.12; quantitative RT-PCR fold change, 0.14).

Additionally, we examined the expression levels of known PTTG1-related genes, including *bFGF* (bead-array fold change, 0.93; quantitative RT-PCR fold change, 0.96) and *VEGF* (vascular endothelial growth factor; bead-array fold change, 0.97; quantitative RT-PCR fold change, 1.02). This analysis revealed that PTTG1 down-regulation in HSA/c and KYSE140 cells did not alter the mRNA expression levels of *bFGF* and *VEGF*. Moreover, ELISA assays confirmed that PTTG1 knockdown treatment did not alter bFGF secretion levels in HSA/c and KYSE140 cells (HSA-LF+, 41.3 ± 4.2 pg/mL; HSA-NTC, 36.0 ± 6.4 pg/mL; HSA-P1, 41.2 ± 2.6 pg/mL; HSA-P2, 41.4 ± 3.2 pg/mL; KYSE140-LF+, 34.9 ± 7.1 pg/mL; KYSE140-NTC, 38.4 ± 4.5 pg/mL; KYSE140-P1, 37.4 ± 4.7 pg/mL; and KYSE140-P2, 37.3 ± 9.1 pg/mL; average value ± SD, not significant).

Discussion

Several studies have shown that PTTG1 expression in primary tumors is associated with metastasis (5–7). However, biological evidence based on animal experiments has not yet clarified the relationship between PTTG1 and cancer metastasis. In the current study, to our knowledge for the first time, we have shown that overexpression of PTTG1 in ESCC cells increases cell motility and promotes lymph node metastasis based on *in vitro* and *in vivo* functional assays.

Overexpression of PTTG1 protein was a frequent event in ESCC primary tumors and cell lines (Table 1*A*; Fig. 2*A*). This finding confirmed the observation in previous studies that PTTG1 is implicated in the development, progression, and lymph node metastasis of breast, gastric, and esophageal cancers (5–7). Our PTTG1 protein expression data in 113 tumors were compatible with these results. In the current study, protein levels of PTTG1 were associated with the presence of lymph node metastases in ESCC. In addition, PTTG1 expression was a significant survival predictor in univariate analyses, whereas PTTG1 was not an independent predictor by multivariate analysis. Because lymph node status is strongly associated with PTTG1 expression level and patient survival (Table 1*A* and *B*), PTTG1 expression may contribute to poor patient survival (Fig. 1*B*) by promoting lymph node metastasis.

PTTG1 protein expression was observed in both the cytoplasm and nucleus in ESCC primary tumors and cell lines. In contrast, PTTG1 was localized only to the nucleus in normal esophageal epithelial cells, particularly in the proliferative esophageal epithelial layer just above the basal cells (Fig. 1*A*). Western blotting using subcellular fractionated samples (Fig. 2*B*) confirmed this immunohistochemical finding as well as the findings in other normal cell types (24). This difference in subcellular localization of PTTG1 protein between normal and cancer cells suggests that PTTG1 localized to the nucleus may play a physiologic role in normal cell division, whereas PTTG1 localized

Table 3. Genes differentially expressed after anti-PTTG1 siRNA treatment in HSAVc and KYSE140 cells

Accession no.	Gene symbol	Description; relationship with cancer	*D*-score (bead array-SAM)	Fold change (bead array)	Fold change (quantitative RT-PCR)
Up-regulated genes					
NM_001219	*CALU*	calumenin; calcium-binding protein, down-regulated in metastatic head and neck cancer cells, related to better survival in lung cancer	1.87	1.7	2.25
NM_019558	*HOXD8*	homeobox D8; possible tumor suppressor	1.54	1.17	1.16
NM_006931	*SLC2A3*	solute carrier family 2, glucose transporter/GLUT3; cancer relation unknown	1.27	2.13	1.4
NM_001498	*GCLC*	glutamate-cysteine ligase, catalytic subunit; possible suppressor in breast cancer	1.15	1.65	1.4
NM_001072	*UGT1A6*	UDP glucuronosyltransferase 1 family, polypeptide A6, transcript variant 1; its polymorphism relates to metabolism of nonsteroidal anti-inflammatory drugs and carcinogenesis	1.00	1.65	1.87
NM_003932	*ST13*	suppression of tumorigenicity 13 (heat shock protein 70 interacting protein); down-regulated in colon and gastric cancers	0.89	1.6	1.11
NM_004887	*CXCL14*	chemokine (C-X-C motif) ligand 14; angiogenesis inhibitor, chemotactic factor in dendritic cells	0.81	1.58	2.25
NM_205862	*UGT1A6*	UDP glucuronosyltransferase 1 family, polypeptide A6, transcript variant 2	0.74	1.6	1.87
NM_003246	*THBS1*	thrombospondin 1; possible angiogenic inhibitor	0.65	1.76	1.27
NM_013253	*DKK3*	dickkopf homologue 3; possible suppressor for melanoma	0.58	1.7	1.36
NM_001627	*ALCAM*	activated leukocyte cell adhesion molecule; possible metastasis suppressor in breast cancer	0.54	1.46	1.73
NM_001005340	*GPNMB*	glycoprotein (transmembrane) nmb; possible metastasis suppressor in melanoma	0.30	1.66	1.41
NM_003739	*AKR1C3*	aldo-keto reductase family 1, member C3; possible suppressor in prostate cancer	0.25	2.12	1.87
Down-regulated genes					
NM_004219	*PTTG1*	pituitary tumor-transforming gene 1	−9.34	0.12	0.14
NM_002808	*PSMD2*	proteasome 26S subunit 2; overexpressed in breast cancer	−2.26	0.76	0.85
NM_001416	*EIF4A1*	eukaryotic translation initiation factor 4A, isoform 1; metastasis-associated gene in lung cancer	−1.63	0.72	0.81
NM_004309	*ARHGDIA*	Rho GDP dissociation inhibitor α/RhoGDIα; related to actin cytoskeletal rearrangements, related to poor prognosis in lung cancer	−1.55	0.82	0.92
NM_006270	*RRAS*	related RAS viral oncogene homologue; promotes cell motility and metastasis in cervical cancer	−1.53	0.73	0.7
NM_001665	*RHOG*	ras homologue gene family, member G/ARHG; promotes cytoskeletal reorganization and migration, related to lymph node metastasis and poor prognosis in breast cancer	−1.24	0.86	0.74
NM_004308	*ARHGAP1*	Rho GTPase activating protein 1/RhoGAP1; modulates Rho-mediated signaling pathways through activation of p21-Rho, cancer relation unknown	−1.21	0.85	0.83

(*Continued on the following page*)

Table 3. Genes differentially expressed after anti-PTTG1 siRNA treatment in HSA/c and KYSE140 cells (Cont'd)

Accession no.	Gene symbol	Description; relationship with cancer	*D*-score (bead array-SAM)	Fold change (bead array)	Fold change (quantitative RT-PCR)
NM_003088	*FSCN1*	fascin; actin-bundling protein, promotes cell migration, related to lymph node metastasis in esophageal cancer	−1.13	0.71	0.89
NM_002205	*ITGA5*	integrin, α_5, fibronectin receptor α; related to invasion of bladder cancer	−0.62	0.58	0.73

Abbreviation: SAM, significance analysis of microarrays.

to the cytoplasm may be related to the malignant phenotype. Therefore, it is reasonable to categorize PTTG1 expression levels by cytoplasmic staining of PTTG1 in ESCC cells. In fact, nuclear PTTG1 staining in 113 ESCC tumors did not correlate with any clinicopathologic features, whereas cytoplasmic PTTG1 staining correlated with several clinical parameters. Mechanisms underlying dysregulation in the subcellular translocation of PTTG1 in ESCC cells remain unclear. However, two different siRNAs directed against PTTG1 effectively knocked down both cytoplasmic and nuclear PTTG1 protein expression in ESCC cells.

The process of lymph node metastasis consists of many steps, including tumor enlargement, lymphangiogenesis, migration into lymphatic capillaries, survival in the lymphatic stream, entry into the subcapsular sinus, invasion of the lymph node cortex, and persistent proliferation (25). The endothelium of lymph capillary has overlapping loose junctions and a discontinuous or absent basement membrane, permitting the passage of large biological macromolecules, pathogens, and migrating cells (26). Once tumor cells reach the adjacent lymphatic capillaries (formation of intratumor lymphatic capillaries may be unnecessary; ref. 27), tumor cells migrate into capillary lumina either through open interendothelial gaps or by inducing the opening of closed gaps (18). As clearly shown in Transwell and Matrigel chamber assays with siRNAs against PTTG1, PTTG1 knockdown reduced cell motility, but interestingly, not penetration through the Matrigel layer. This finding suggests that PTTG1 may promote the entry of tumor cells into lymph capillary lumina by increasing tumor cell motility, which is considered an early stage in the multistep theory of lymph node metastasis. Previously, we have shown that cell motility is closely associated with lymph node metastasis and poor survival (14, 18, 28, 29). For example, reduced expression of motility-related protein 1 and overexpression of chemokine (CC motif) receptor 7 were associated with lymph node metastases in ESCCs (28, 29). Similarly, overexpression of fascin, an actin-bundling protein related to cell motility, was significantly associated with regional lymph node metastasis and poor survival in ESCC patients, and down-regulation of fascin in ESCC cells decreased their motility (18). Moreover, overexpression of osteopontin, an integrin-binding secreted glycoprotein associated with cell motility, was significantly associated with distant lymph node metastasis and poor survival of ESCC patients, and knockdown of osteopontin expression in ESCC cells induced by an inducible short hairpin RNA vector decreased their motility, invasiveness, and popliteal lymph node metastasis from footpads of nude mice (14). As shown in the current study, knockdown of PTTG1 expression in ESCC cells by *in vitro* and *in vivo* transfection significantly decreased popliteal lymph node metastases from footpads in nude mice. Thus, PTTG1 may be related to cell motility and lymph node metastasis in ESCC.

To identify potential downstream genes in the PTTG1 pathway, we performed global gene expression profiling using a bead array–based technique and siRNAs directed against PTTG1. As shown in Table 3, siRNAs directed against PTTG1 down-regulated the expression of several Ras and Rho gene family members known to play central roles in cell motility via actin cytoskeleton rearrangement (30). Some of the genes identified by this strategy have exhibited clinical correlation with poor survival or metastasis. *RRAS*, which plays a key role in cell motility by modulating Rho and Rac activities (31), promotes metastasis in cervical cancer (32). *RHOG*, which regulates cell motility through Rac1 activation (33), is related to lymph node metastasis and poor prognosis in breast cancer patients (34). *ARHGDIA*, which acts as an inhibitor of Rho family members, is related to poor survival in lung cancer patients (35). *ARHGAP1* modulates Rho-mediated signaling pathways through activation of p21-Rho (36), but the relationship between *ARHGAP1* and cancer metastasis is unknown. Interestingly, *FSCN1* (fascin), which regulates cell motility through its actin-bundling function, was also down-regulated in our study by siRNAs against PTTG1. In contrast, potential tumor suppressors or metastasis suppressors, including *CALU* (37, 38), *HOXD8* (39), *GCLC* (40), *ST13* (41), and *CXCL14* (42), were up-regulated by PTTG1 down-regulation. *THBS1* (thrombospondin 1), a potential angiogenesis inhibitor, was up-regulated by PTTG1 down-regulation. Consistent with this result, Kim et al. (43) reported that *THBS1* expression was suppressed in PTTG1-overexpressing thyroid cells, and that down-regulation of PTTG1 increased THBS1 expression. *THBS1* also predicts poor survival and represents a marker of tumor aggressiveness in thyroid cancer (44). *bFGF* and *VEGF*, which are known PTTG1-related genes, were also included in the gene list derived from our expression profiling. However, their expression levels did not change after PTTG1 knockdown in our experimental setting. Thus, cell motility regulated by PTTG1 could be independent of bFGF or VEGF in ESCC cells. Taken together, these microarray results suggest that PTTG1 may modulate the expression of multiple cell motility–related genes, including Ras-Rho oncogene superfamily members, and provide potentially valuable clues